Real-Time Automated Tracking and Trapping System for Sperm

LINDA Z. SHI,[1] JACLYN NASCIMENTO,[2] CHARLIE CHANDSAWANGBHUWANA,[1]
MICHAEL W. BERNS,[1,3,4] AND ELLIOT L. BOTVINICK[4]*
[1]*Department of Bioengineering, University of California at San Diego, La Jolla, California 92093-0435*
[2]*Department of Electrical and Computer Engineering, University of California at San Diego, La Jolla, California 92093-0407*
[3]*Department of Biomedical Engineering, University of California at Irvine, Irvine, California 92612-2715*
[4]*Beckman Laser Institute, University of California at Irvine, Irvine, California 92612*

KEY WORDS laser tweezers; sperm motility; automatic tracking and trapping; video rate

ABSTRACT We have developed a microscope system for real-time single sperm tracking with an automated laser tweezers escape power assay. Phase contrast images of swimming sperm are digitized to the computer at video rate. The custom algorithm creates a region of interest centered about a sperm in response to a mouse click and performs all subsequent tasks autonomously. Microscope stage movement responds to feedback from video analysis of swimming sperm to center the sperm with respect to the field of view. For escape power assays, sperm are automatically relocated to the laser trap focus where they are held for a user-defined duration at fixed power, or held as laser power is gradually reduced. The sperm's position is automatically monitored to measure the laser power at which the sperm escapes the trap. Sperm are tracked for extended durations before and after laser trap experiments. Motility measurements including the curvilinear velocity and the absolute position of the sperm relative to the cell chamber are calculated and written to the hard drive at video rate. Experimental throughput is increased over 30 times compared to off-line data analysis. The efficacy of the "track and trap" algorithm is validated through examples and comparisons with the manually collected data. *Microsc. Res. Tech. 69:894–902, 2006.*

INTRODUCTION

Real-time computer-based tracking of live cells has become an important tool in cell biology. Berns and Berns (1982) developed an edge detection algorithm that operated in combination with robotic feedback control of the *x*-*y*- and *z* microscope planes to follow the movement of living mammalian cells while keeping them centered in the field of view. In that study, the maximum cell velocity was 30 μm/h. In a subsequent study on amphibian eosinophils (Koonce et al., 1984), maximum cell velocity was 31 μm/min. Poole et al. (1988) developed a computerized image processing system to track individual free-swimming cells and rotating bacterial cell bodies tethered by their flagella, in real-time. Cells were imaged at 50 frames/s in a fixed field of view with a maximum analyzed cell speed of 120 μm/s. Their system utilized a fixed threshold method to identify cells and terminated tracking if cells went out of focus, crossed paths or reached the edge of the screen. Rabut and Ellenberg (2004) proposed an algorithm for automatic real-time 3-D cell tracking by fluorescence microscopy. Multiple cells were tracked simultaneously with a maximum cell speed of 10 μm/s. Sage et al. (2005) presented a Java plug-in application for ImageJ software to track the movement of chromosomal loci within nuclei of budding yeast cells. The images were aligned to compensate for the movement of biological structure, the particle's signature was enhanced, and the optimal trajectory of the particle was extracted in the algorithm. Our recent studies have been focused on tracking sperm. These cells move with velocities of hundreds of microns per second, thus presenting unique challenges for accurate computer-assisted sperm analysis (CASA). These challenges relate not only to the speed with which the sperm changes position, but also with respect to changes in the pixel distribution and intensity over time. Thus the development and use of CASA has become a major research focus in clinical andrology and sperm research (Amann and Katz, 2004; Mortimer, 1994; Stephens et al., 1988). Notwithstanding the high level of interest, CASA systems generally are limited in the maximum number of consecutive frames that can be analyzed at video rates. Young et al. (1996) developed a real-time sperm tracking system with unlimited frame number that monitored a single sperm entering a fixed microscope field. Kuo et al. (2000) extended this research and developed an automated-stage sperm tracking system (ASTS) designed to analyze highly dilute sperm suspensions at 30 frames/s. The human sperm velocities presented in that paper were less than 50 μm/s, which is much less than the hyperactivated sperm defined in Neil and Old-Clarke (1987) and Mortimer (1997). ASTS was reported to fail for sperm with "high speed and large-angle zig," i.e., for sperm with

*Correspondence to: Elliot Botvinick, Beckman Laser Institute, 1002 Health Sciences Road East, Irvine, CA 92612, USA. E-mail: elliot.botvinick@uci.edu

Received 16 March 2006; accepted in revised form 24 May 2006

Contract grant sponsor: Air Force Office of Scientific Research; Contract grant number: AFOSR F9620-00-1-0371; Contract grant sponsor: Beckman Laser Institute Inc. Foundation.

DOI 10.1002/jemt.20359

Published online 4 August 2006 in Wiley InterScience (www.interscience.wiley.com).

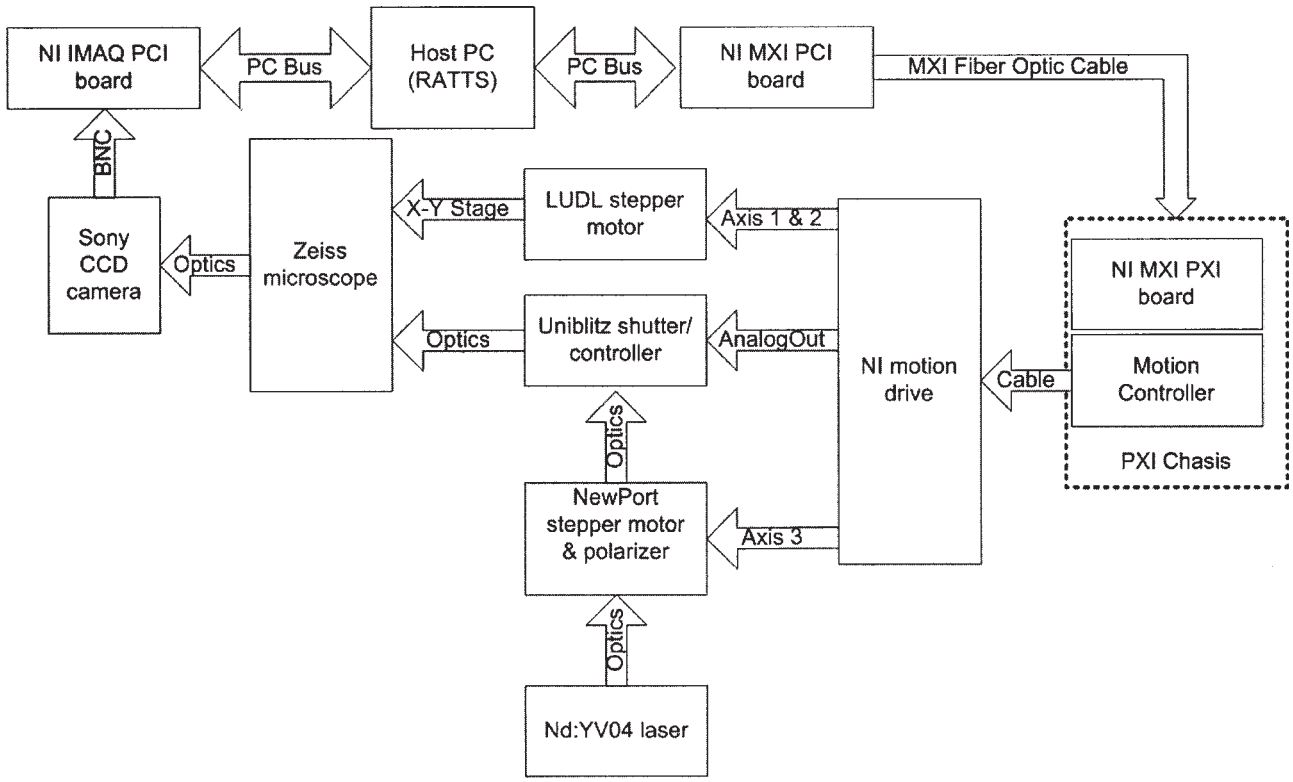

Fig. 1. Block diagram of hardware.

high curvilinear velocity (VCL) and large lateral head displacement during swimming.

To expand the automated measurable parameters of sperm motility we developed a system that can measure both the force with which individual sperm swim as well as swimming speed (VCL). In these studies optical tweezers were used to measure the sperm swimming force (Konig et al., 1996; Lang and Block, 2003; Nascimento et al., in press; Tadir et al., 1989). To accomplish this, the sperm-of-interest was initially positioned into the laser trap using a manual joystick that controlled the x-y microscope stage movement. Additionally the user recorded digital images of the sperm for a period before and after trapping in order to have data for off-line analysis. A robust single sperm tracking algorithm (SSTA) was developed (Shi et al., Computer-based tracking of single sperm, submitted) for this application. While SSTA circumvented the errors observed in existing commercial CASA tracking systems, it had the drawback of low experimental throughput. In addition, saved images needed to be reviewed repeatedly in order to: (1) confirm the identity of the trapped sperm, (2) identify the first image frame of the trapped sperm after the cessation of stage movement, (3) identify the last image frame before the stage was moved to place the sperm in the laser trap, (4) identify the first image frame post sperm escape from the trap, and (5) identify the last image frame before the next sperm trapped.

In this study we describe a real-time automated tracking and trapping system (RATTS) that operates at video rate. After initially identifying and clicking the computer mouse on the sperm of interest, RATTS performs all further tracking and trapping functions without human intervention.

MATERIALS AND METHODS

System Hardware Control

Figure 1 shows a block diagram of the hardware. The optical system and specimen preparation have been detailed previously (Nascimento et al., in press). Briefly, cryogenically frozen dog sperm were thawed and suspended at 30,000 sperm per milliliter of Biggers, Whittens, and Whittingham media. Suspensions were injected into 2 mm deep cell culture chambers (Rose chambers). A Nd:YVO4 continuous wave 1,064-nm wavelength laser (BL-106C, Newport Corporation, Irvine, CA) is focused into a Zeiss Axiovert S100 microscope equipped with a 40× [phase III, NA 1.3] oil immersion objective (Zeiss, Thornwood, NY). The laser creates a single-point 3-D gradient laser trap. The host computer contains an ASUS P5AD2 mother board supporting an Intel Pentium 4 CPU (3.4 GHz, 1 MB L2 onboard cache) with an 802.8-MHz bus and 2-GB RAM. Two hard drives (IDE, 36 GB, 8 MB onboard cache, 7,200 RPM, Western Digital, Lake Forest, CA) were connected through the motherboards' RAID level 0 controller configured for data striping with a block size of 64 kB. An image acquisition board (NI PXI-1407, National Instruments, Houston, TX) is housed in the host computer to digitize analog video signals. A 7344 motion controller (7344, National Instruments) is housed in a PXI chassis (NI PXI-1000B, National

Instruments) which is controlled from the host PC through a MXI-3 link connected with a fiber-optic cable. A MXI-3 PCI interface card (PCI 8335, National Instruments) in the host computer transmits/receives data to the MXI-3 PXI card in the PXI chassis (PXI 8335, National Instruments) through a bidirectional fiber-optic cable, thereby implementing a PCI-PCI bridge. A 4-axis stepper-motor driver (MID-7604, National Instruments) connected to the motion controller drives the x-y stepper-motor stage (LUDL Electronic Products, Hawthorne, NY) of the microscope. Video signals from an RS-170 standard CCD camera (Model XC-75, Sony, Japan) are distributed to a TV monitor, a Camcorder (Sony, Japan) for recording, and the image acquisition board through a video distribution amplifier (not shown) (IN3218HR, Extron Electronics, Anaheim, CA). A mechanical shutter (Uniblitz LS6ZM2, Vincent Associates, Rochester, NY) in the laser path is controlled by a shutter driver (Uniblitz VMM-D3, Vincent Associates) through two lines of digital input–output from the motion controller. A rotary stepper motor mount (PR50PP, Newport Corporation) housing a Glan laser linear polarizer is controlled by the motion controller and stepper motor driver to modulate power in the laser trap.

Video Rate Tracking With Automated Stage Control

A key feature of RATTS is the ability to track sperm at video rates and to update the microscope stage position to keep a swimming sperm in the field of view. RATTS is custom coded in the LabView 7.1.1 language (National Instruments) to process streaming images, calculate sperm trajectories, and drive the motion hardware. RATTS implements the image segmentation and sperm tracking algorithm (SSTA) previously described (Shi et al., Computer-based tracking of single sperm, submitted). SSTA uses contrast enhancement and multi-class image segmentations to extract sperm swimming with transient focal quality. These methods are necessary, as the depth of field of the high NA (1.3) microscope objective is on the order of the sperm head size. The transient focal quality, due to axial head motion or altered axial position of the sperm, yields transient contrast and brightness as compared with other objects in the field, including neighboring sperm. As an improvement over commercial CASA systems, SSTA recognizes sperm collisions and uses its postcollision analysis to statistically recover the tracked sperm. A postcollision analysis is trained with noncolliding sperm trajectories to statistically determine the probability of deviating from mean swimming behaviors. These probabilities determine the likelihood of sperm pairing between pre- and postcollision sperm.

Images are digitized by the image acquisition board and transferred into a continuous buffer from which they are retrieved for image analysis and displayed in the front panel (Graphical User Interface in LabView). Image analysis detects when a tracked sperm has reached a rectangular boundary near the extremity of the camera field of view (about 52% percent of the field). RATTS moves the microscope stage to position the calculated sperm centroid into the center of the field. In one mode of operation the sperm centroid position is extrapolated to predict the sperm's position beyond the most recent image in order to compensate for swimming during the stage movement. Swimming parameters are calculated and saved in a continuously updated data file. Since new images arrive at the rate of 30 frames/s, it is necessary to restrain net computation and data writing time to less than 33 ms in order to capture and process each image. RATTS is coded to use the most recent frame in the buffer, and consequently, if image analysis time is more that 33 ms an image will be skipped and the next image will be processed. To benchmark RATTS performance, skipped frames were documented and process times were benchmarked using LabView's timing tools. Sperm were recorded and tracked for extended durations to demonstrate variability in swimming parameters and variation in VCL as a function of track length and integration interval.

Tracking and Trapping

The automated trapping feature of RATTS replaces the manual protocol previously described (Nascimento et al., in press). User input is limited to setting parameters prior to an experiment and selecting, via the computer mouse, a sperm in the field for analysis. The user enters the number of image (to be captured and stored) frames to analyze prior to and posttrapping. The user can select the method of laser exposure: (1) laser power is held constant for a fixed duration in the trapping phase of the experiment or (2) laser power is decayed during trapping. Parameters are entered for maximum (or constant) laser power, rate of power decay, and if appropriate, duration of the trap. During the experiment, the user selects a sperm to be analyzed by clicking on its image with the arrow cursor on the front panel of RATTS. The cursor coordinate is registered, passed to the tracking algorithm, and computation proceeds with no further intervention. Once the specified number of frames have been processed, the stage is moved to place the sperm under the laser trap and the shutter is opened.

In one mode of operation (selected prior to the experiment) the stage update can be performed iteratively a few times before the trap is opened. Since image analysis does not occur during stage movement, errors in the sperm position arise from sperm swimming during that movement and from positioning errors inherent in the rotary-encoded stepper motor stage. If the sperm center is not adequately aligned with the laser focus, the scatter force of the trap will push the sperm out of focus and the sperm will be lost. After the first stage movement, subsequent movements are relatively rapid as the sperm is already near its target position. As mentioned previously, a predictor may also be used to predict the post stage translation position of the sperm.

During the trapping phase of the experiment, RATTS implements an escape detection subroutine to detect the presence of a sperm in the laser trap and to respond if the sperm escapes the trap. The subroutine monitors a small square pixel region (representing ~10 μm/side) centered about the laser trap. Using SSTA, the subroutine segments the image within this region and uses a size threshold to detect the presence or absence of a sperm. A sperm must remain in the trap

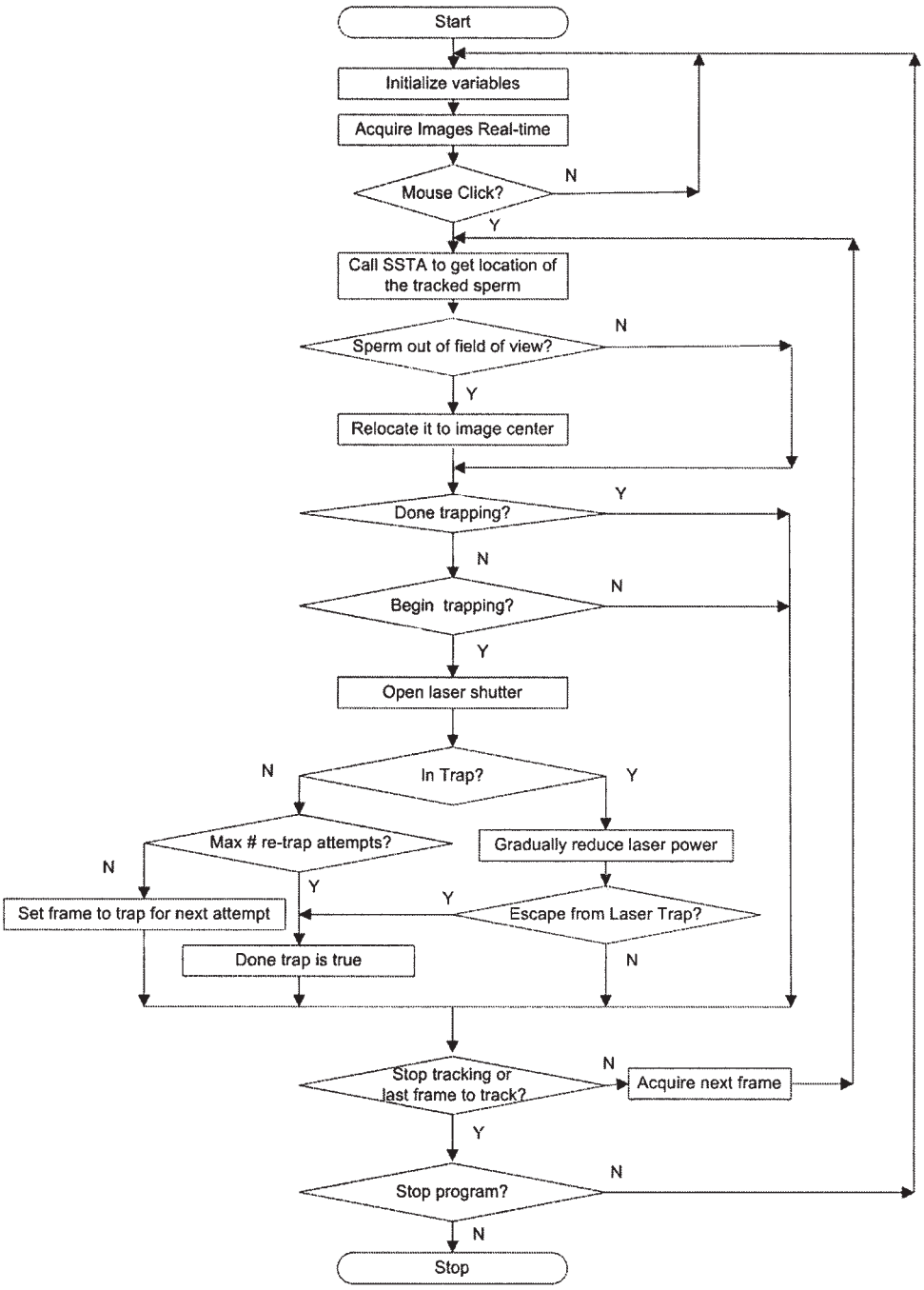

Fig. 2. Flowchart of RATTS during power decay experiments.

for a continuous 15 frames or the subroutine declares a failed trapping attempt.

Tracking and Trapping—Constant Power

During constant-power trapping experiments the escape detection subroutine is used to ensure that first, the sperm was successfully trapped, and second, that it does not escape the trap during the trapping phase of an experiment. If the sperm prematurely escapes the trap, then RATTS will use SSTA to find the sperm and continue tracking it for a user-defined number of frames after which a new trapping attempt is made. RATTS will repeat this either until the sperm is trapped, or for a user-defined number of attempts.

Tracking and Trapping—Power Decay

In power decay experiments, the escape detection subroutine as described in the previous section is used to ensure that a sperm is stably trapped. The laser power used to first trap a sperm is a user-defined percentage of maximum power (or maximum transmission through the polarizer). RATTS automatically decays

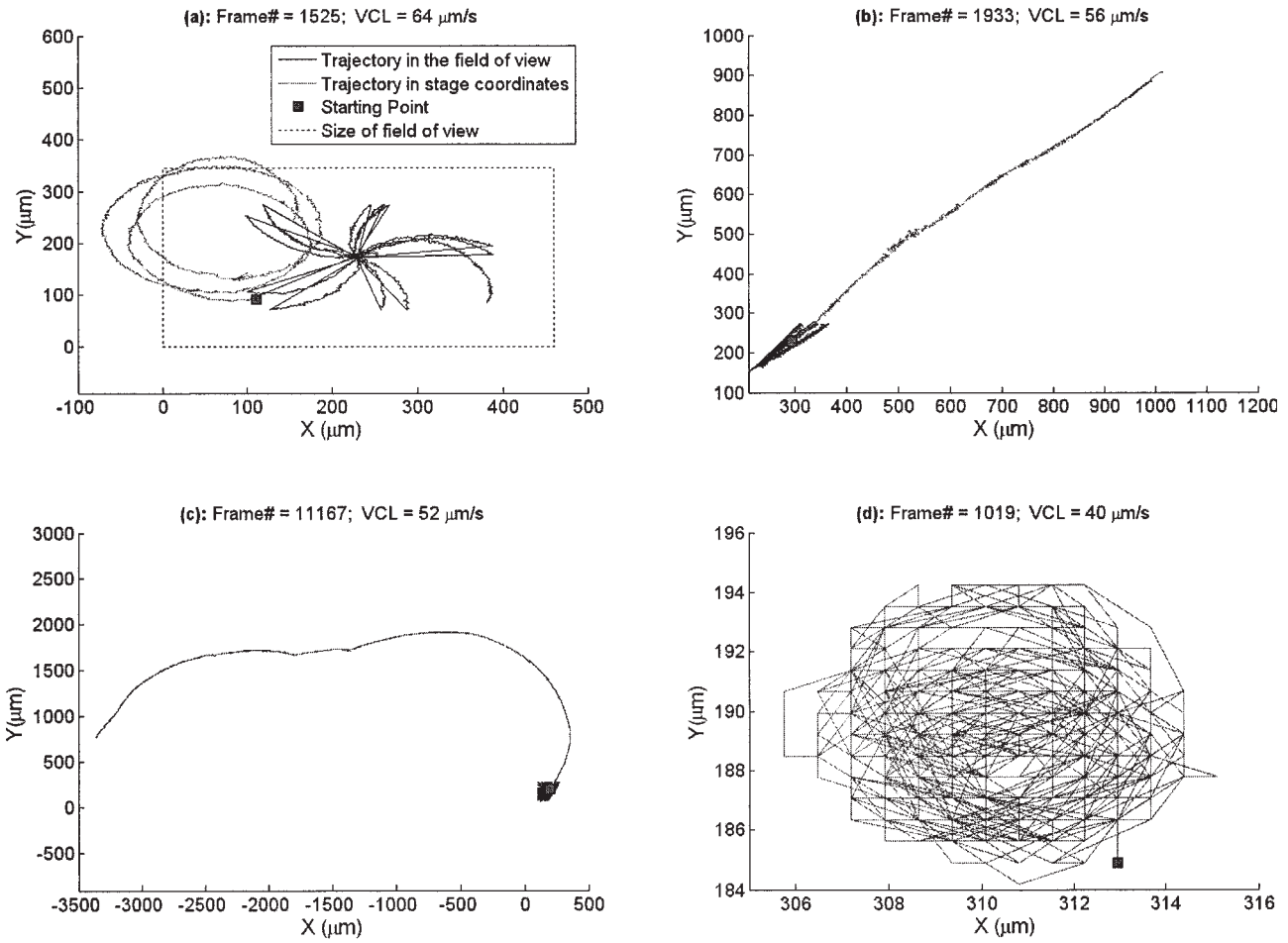

Fig. 3. Trajectories from real-time continuously tracked dog sperm. Continuous tracks are plotted for both stage (gray lines) and field-of-view (solid lines) coordinates. Straight-line black segments represent stage movements. For each trajectory the number of consecutive frames (Frame#) and the VCL are shown. (**a**) A sperm swimming in a circle of radius greater than the rectangular boundary used to trigger stage movement (not shown, about 52% of the field of view), (**b**) a sperm swimming in a near straight line, (**c**) a sperm moving in a straight line over short distances, but in a curved trajectory over millimeters, and (**d**) a sperm with a portion of its tail adhered to the glass coverslip, spinning about itself (commonly assigned a motility score of SOP 1*).

the laser power by rotating the polarizer. Decay parameters such as speed of decay, max/min laser power, and time until complete decay are all user defined. Once an escape is detected, the polarizer position (and thus laser power) is written to disk and the polarizer is automatically rotated back to its starting position. A running file is updated at video rate to record real-time swimming parameters, including frame-by-frame centroid coordinates, position, and escape power. Figure 2 shows a flow diagram of the RATTS algorithm for power decay experiments.

To compare escape power measurements between the automatic assessment using RATTS and the manual assessment in Nascimento et al. (in press), a subroutine was written to record the position of the polarizer when the user clicks an on-screen button after observing an escape event. Meanwhile RATTS computationally determines the moment of escape and the corresponding polarizer position. The power decay continues until both RATTS and the user respond to the escape event. Latency in the human response can result in power measurement biased towards a lower power determination, since the polarizer continues to rotate during the period between observation and the mouse click.

RESULTS

The sperm detection subroutine, which includes image contrast enhancement, image thresholding (single level), and particle analysis is processed in 1–8 ms. Processing only increases to 1–9 ms when the multithreshold algorithm is engaged (i.e., when a second sperm enters the pixel region surrounding the sperm (Shi et al., Computer-based tracking of single sperm, submitted)). Reading the position of the polarizer during power decay takes 1–2 ms. Thus the total per-frame processing time is less than 11 ms, and the image processing time can keep up with the image acquisition rate. Processing time and motor actuation to relocate the tracked sperm either to the center of the field of view or under the laser trap is typically 25–39 ms. This typically results in the loss of one image at 30-Hz video rate.

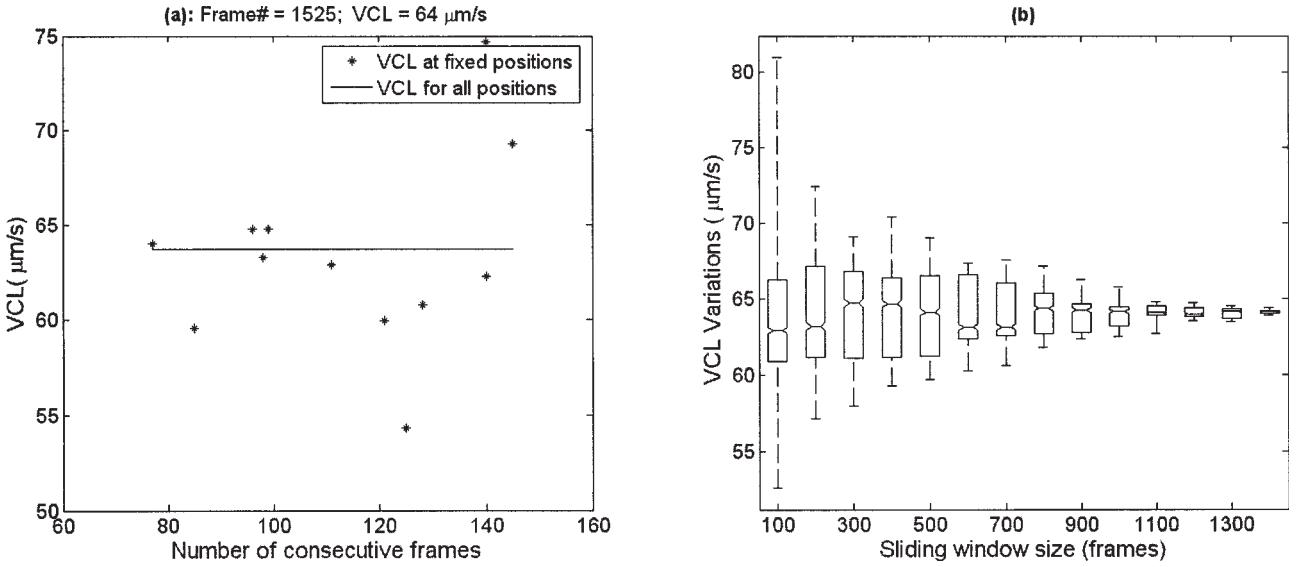

Fig. 4. Variability in VCL of a single dog sperm between fields of view (and thus with time). (**a**) A field-by-field analysis of the long-range track shown in Figure 3a. The VCL is plotted as a function of the number of consecutive image frames tracked for each static stage position. The solid line indicates VCL calculated across all stage positions. (**b**) Box plot of VCL for the track shown in Fig. 3a as a function of averaging window size. At 100 frames wide the distribution is wide with extreme outliers. VCL is mainly distributed the same for windows 100–500 frames wide, and the distribution narrows significantly for windows over 1,000 frames wide.

Figure 3 plots the trajectories of four different sperm which have been tracked for as many as 11,167 consecutive video frames. Figure 3a shows the trajectories with respect to a fixed field of view and as a montage spanning all stage positions. Figures 3b and 3c demonstrate the global nonlinearity of sperm swimming which may appear relatively straight when viewed in a stationary field. Figure 3d demonstrates continuous tracking of a sperm that is stuck to the glass, commonly assigned a speed of progression (SOP) of 1.

Figure 4 shows the variability in VCL for the sperm trajectory in Figure 3a. Figure 4a plots the VCL calculated during each fixed stage position as the sperm moved through the field of view. The mean VCL observed was 64 μm/s with 15% maximum deviation. For the same trajectory, Figure 4b contains a box plot representing the distribution of VCL calculated with sliding windows of various lengths (100, 200,. . .,1500). While the median (the horizontal line within each box) values change between widow lengths 100–500, the box size (containing the central 50% of the data) and position remain fairly consistent. Further increasing the shifting window length tightens the distribution, indicating a statistically stationary distribution.

Figure 5 demonstrates real-time sperm tracking with trapping at constant laser power. Sperm were trapped for 200 video frames (6.67 s) at 350 mW laser power. Each of the four subfigures demonstrates: (1) tracking a single sperm over multiple fields of view prior to trapping, (2) moving the stage to trap the sperm for 200 video frames, and (3) continuation of tracking posttrapping.

Figure 6 shows errors in the measurement of escape power when manual assessment (by pressing a button in RATTS) is used as opposed to RATTS automatic assessment (escape detection subroutine in RATTS). Error is defined as the RATTS' measurement minus the manual measurement. Manual measurements were less than or equal to those of RATTS 95% of the time. Delay times between RATTS' and manual detection of escape had a mean and standard deviations of [0.46, 0.4] seconds, with delays as long as 3 s. Scatter plots (not shown) of error against either VCL or the RATTS' measurement show no nonlinear relationship. Linear regression of errors as a function of VCL yields slope = 0.06, $R^2 = 0.04$, $P = 0.1$, which casts doubt on a nonrandom relationship. Linear regression of errors against the RATTS measurement yields slope = 0.02, $R^2 = 0.05$, $P < 0.05$, which indicates a very weak relationship, if any, with poor predictive power. Thus manual measurements cannot be corrected retrospectively.

Figure 7 summarizes the results of a side-by-side power decay experiment comparing RATTS with the previous manual method (Nascimento et al., in press). Both methods identify three groups within the plot: (1) having low power at low VCL (SOP 2*), (2) having escape power (P_{esc}) and VCL correlated (SOP 3*), and (3) having outlying sperm that escape at higher laser power (>150 mW) than other sperm with the same VCL. Escape powers within each group were not normally distributed. A Wilcoxon rank sum test with an equal median null hypothesis found the manual and RATTS' power measurements to be significantly similar within each group ($P > 0.05$). It can be concluded that the automation of RATTS produces similar, if not more accurate, data to the manually driven protocol.

DISCUSSION

The algorithm and hardware integration presented in this study have achieved fast, automated sperm motility analysis with automated laser tweezers force measurements. Reducing image processing time within video rate operation was the key feature enabling RATTS' real-time sperm tracking. With respect to the

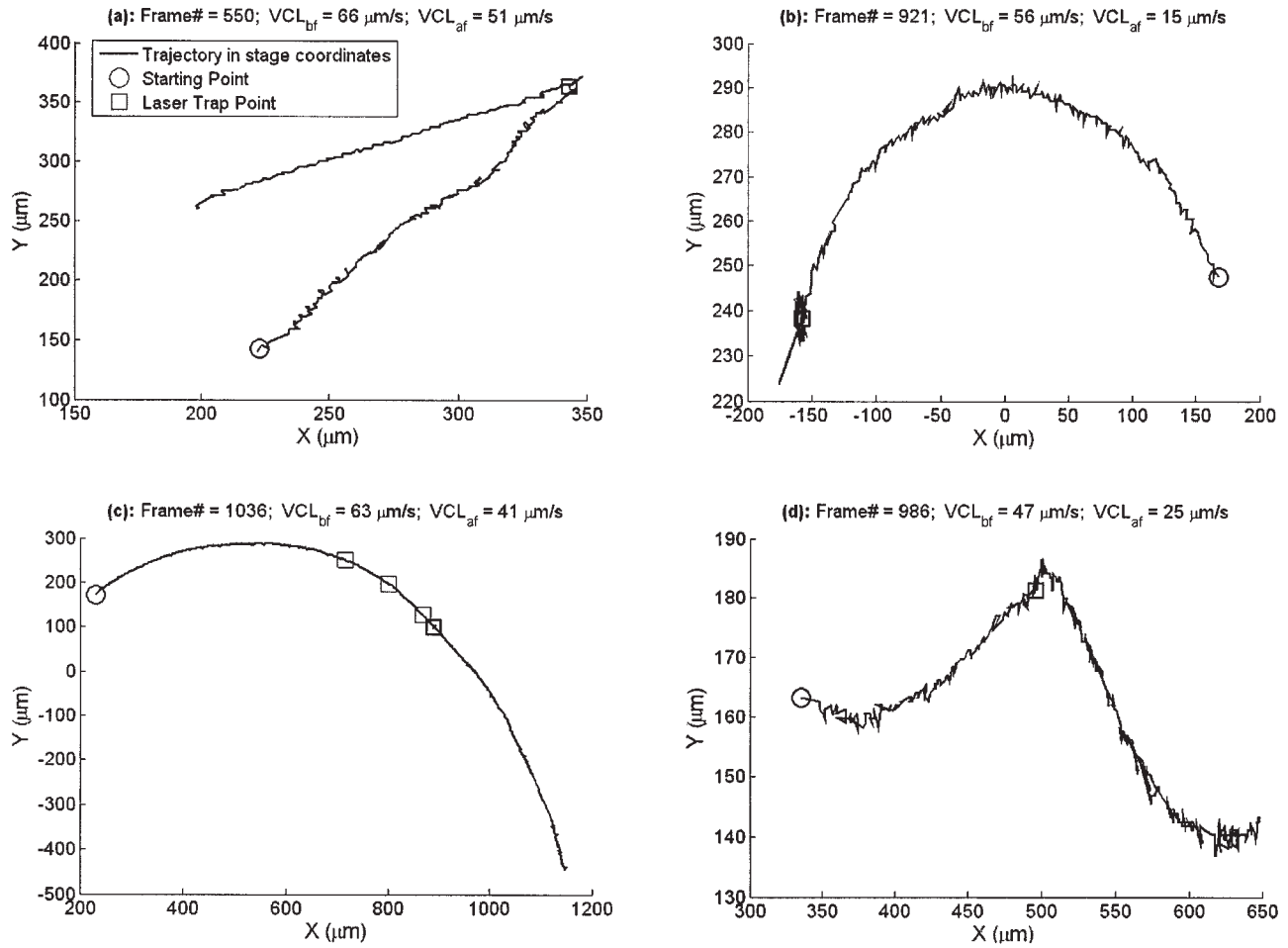

Fig. 5. Trajectories from real-time continuously tracked dog sperm with laser trapping at constant power (350 mW for 6.67 s). For each trajectory the starting point (○) and the trapping location (□) are shown as well as the number of frames tracked (Frame#), VCL before (VCL_{bf}), and VCL after (VCL_{af}) trapping. (**a**) A sperm swimming along a straight trajectory changes swimming direction after laser trapping and (**b**) a sperm swimming in a large arc before and after trapping with no significant trajectory change. Three failed attempts to trap are indicated by thin squares. RATTS automatically detected the failed attempts, continued to track, and attempted trapping again until the sperm was stably trapped (thick square). (**c**) Sperm spinning out of trap, stabilizing, and swimming along new trajectory nearly perpendicular to original and (**d**) sperm escaping the trap at half of the VCL at which it entered.

LabView programming language, we found that reducing our dependency on local variables and replacing them with shift registers decreased RATTS' computation time by 5–8 times. With respect to computer hardware, we found that implementing data stripping in a RAID level 0 array was necessary to achieve video rate operation. Before RAID was enabled, we found that, on average, the sum of our subroutine times was greater than the maximum allowable 33 ms. In its current configuration, RATTS needs 11 ms calculation time and should be able to accommodate up to 90-Hz frame rates which are sufficient to capture the side to side head motion of hyperactive human sperm (Mortimer, 1997). For the case of dog sperm, Corral-Baques et al. (2005) reported the beat cross frequency (BCF) to be 15 Hz. The BCF is the frequency of lateral head movements about the mean path of the sperm. According to the Nyquist sampling theory, sperm must be imaged at twice the BCF in order to avoid aliasing and thus decreasing VCL values. RATTS samples at 30 Hz, which just satisfied nyquist sampling for dog sperm. We are currently integrating an 80-Hz camera into RATTS in order to oversample dog sperm and to experiment on other species with higher BCFs.

As can be seen in Figure 3, RATTS' real-time tracking can follow sperm swimming in a variety of patterns, be it the circle swimmer of Figure 3a, the straight swimmer of Figure 3b, or the meandering sperm of Figure 3c. Clearly, a few seconds is not sufficient time to identify the swimming pattern of each sperm. By tracking at video rate and updating the stage position to retain the sperm within the field of view of the camera, RATTS allows long duration examination of the swimming pattern. For example, the sperm of Figures 3a–c are tracked for 51 s, 64 s, and 6.2 min respectively. Clearly any 100-frame sequence along those trajectories would be insufficient to adequately describe them. Little is known of the purpose or physiological implications of sperm swimming pattern, but with systems such as RATTS, swimming patterns can be studied in an array of experimental protocols, including the measurement of swimming force.

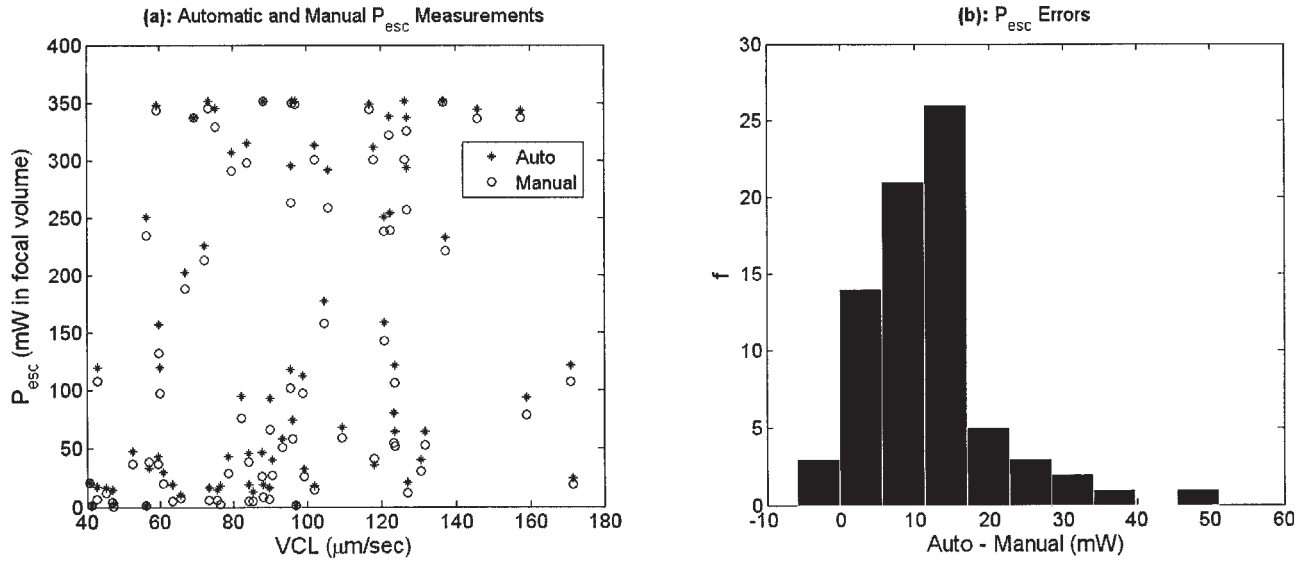

Fig. 6. Comparison of measuring escape power (P_{esc}) manually and automatically. (**a**) Scatter plot showing escape power (P_{esc}) measured automatically by RATTS (*) and manually by user mouse click (○) for 76 sperm representing a wide range of VCLs. (**b**) Histogram of P_{esc} error, defined as the automatic P_{esc} measurement minus the manual P_{esc} measurement for each sperm. Manual measurements reported lower escape power 95% of the time. This is likely due to latency in the human response as the polarizer continues to rotate. No correlation was found between P_{esc} error and either RATTS' estimate of P_{esc} or VCL, thereby thwarting retrospective correction of manual P_{esc} measurements.

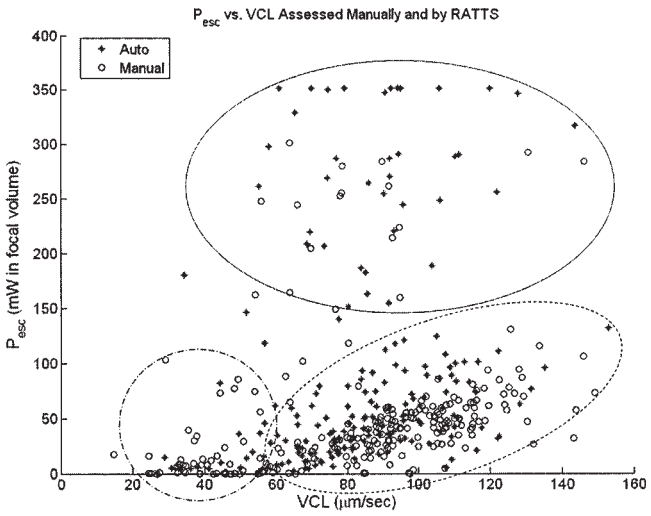

Fig. 7. Results from power decay experiments demonstrate that RATTS is a suitable substitute for manual analysis of sperm motility and laser power experiments. Data were collected manually with off-line SSTA analysis (×) and automatically with RATTS (○). Mixed sperm from multiple dogs were thawed from cryogenic storage and tested. The two data sets represent different mixtures of dog sperm. Three classes of sperm are identified by both methods, as circumscribed in the figure: those swimming with a linear relationship between VCL and P_{esc} (– –), low VCL swimmers with no linear relationship to P_{esc} (— ·), and an outlier group with statistically greater P_{esc} than those in either of the first two groups (—). Sperm were collected and handled according to Nascimento et al. (in press).

It is important to point out that RATTS does not measure force directly. The swimming force of a sperm escaping the laser trap is proportional to the laser power and can be described by the equation: force = $Q \times n/c \times P_{esc}$, where n is the index of refraction of the media and c is the speed of light. The trapping efficiency, Q, is a dimensionless variable dependent on wavelength, NA, beam shape, chamber depth, and heavily upon geometry of the sperm. The swimming force corresponds to the maximum value of Q, as a trapped sperm is moved relative to the trap. Konig et al. (1996) measured Q for human sperm by the viscous drag test, measuring trapped sperm heads after their tails were removed by laser scissors. Q was determined with 16% error. Each species measured by RATTS will need to be similarly calibrated in order to calculate Q. As the method is described in earlier work, only escape power is reported in this study.

The addition of laser escape power measurements has revealed the presence of an outlying ubiquitous group of sperm that escape at higher laser power (and thus trapping force) than other sperm in the same population that are swimming with similar VCL (Nascimento et al., in press). The automation offered by RATTS has allowed us to investigate the nature of the outlying sperm by removing the inefficient manual method of control and analysis. Additionally, RATTS allows us to examine not only the swimming speed–escape power relationships, but also the effects that the trap may have on the swimming sperm. Figure 5 demonstrates four different responses to a laser trap of constant power and duration. In Figure 5a, a sperm leaves the trap at a radically different angle and at 77% of the VCL at which it entered. It can be seen that the lateral component of swimming decreased considerably. In Figure 5c the sperm's swimming pattern is unaltered, but the VCL decreases by 35%. Three trapping attempts failed before the sperm was stably trapped. Stable trapping requires the laser focus to overlap the sperm head. Any change in focus or swimming pattern in the few frames around the trapping attempt

may lead to an unsuccessful trap. Success rates may improve with head trajectory prediction, but as is, most trapping attempts succeed on the first try. The sperm in Figure 5d exited the trap along the same trajectory as it entered, spinning about its head, and then straightening out to swim nearly perpendicularly and at 53% of the VCL. The sperm in Figure 5b exited the trap at a relative crawl (25%) compared to the VCL at which it entered. Whether these effects are physiological or experimental artifacts remains unclear. The four examples here all show sperm slowing down by at least 23% after trapping, which does not represent the general trend. As a population, Nascimento et al. (in press) found that, on average, dog sperm trapped at 350 mW for 5 s escaped at 93% (1.4% standard deviation) VCL prior to trapping. Instead, the examples were chosen to demonstrate the capabilities of RATTS. The study of sperm swimming before, during, and after laser trapping may unlock new understanding regarding sperm–light interactions and sperm mechano-sensitivity.

RATTS also addresses the inaccuracy introduced by manual assessment of escape power, as shown in Figure 6. Since previous work (Nascimento et al., in press) determined the maximum time a sperm can be held in the trap without damage, it is necessary to reduce laser trapping power rapidly enough to eliminate any damage effects caused by the trap. As such, the laser power decay occurs in about 10 s. At this rate of decay, any latency between the sperm escape and the computer's recognition of it will lead to an underestimate of escape power as the polarizer will continue to rotate during the period of latency. During manual assessment of laser power such latency was significant and random with respect to VCL and laser power. As such, the manual measurements cannot be retrospectively corrected. RATTS circumvents this latency error through its automated detection of escape and near instantaneous cessation of polarization rotation.

RATTS' data were found to be comparable to the manually collected data (latency error aside). Both techniques identify the three groups of sperm (SOP2*, SOP3*, and outliers) previously described (Nascimento et al., in press), as shown in Figure 7. Statistical analysis shows that the three groups found by each technique are likely from identical distributions. Since both analyses were done on sperm from the same species, it can be concluded that both methods offer the same experimental data. RATTS offers two critical improvements: increased throughput and more accurate power determination.

In summary, RATTS is capable of tracking single sperm well beyond the limits of a fixed field of view. The microscope stage movement is rapid enough to lose only a single frame during each field of view update. The long-range tracking allows RATTS to gather **s**tatistically significant swimming data before and after the sperm is trapped by the laser. In addition, RATTS' continuous operation has enabled identification and typically tracking of SOP 1 (nonswimming) sperm which are not detectible by the automated CASA systems. In conclusion, we have developed a highly automated sperm tracking and trapping system that has high throughput and which provides motility measurements of both velocity and swimming force. RATTS can easily be extended to the study of other motile cell types.

REFERENCES

Amann RP, Katz DF. 2004. Reflections on CASA after 25 years. J Androl 25:317–325.

Berns GS, Berns MW. 1982. Computer-based tracking of living cells. Exp Cell Res 142:103–109.

Corral-Baques MI, Rigau T, Rivera M, Rodriguez JE, Rigau J. 2005. Effect of 655-nm diode laser on dog sperm motility. Lasers Med Sci 20:28–34.

Konig K, Svaasand L, Liu Y, Sonek G, Patrizio P, Tadir Y, Berns MW. 1996. Determination of motility forces of human spermatozoa using an 800 nm optical trap. Cell Mol Biol (Noisy-le-grand) 42:501–509.

Koonce MP, Cloney RA, Berns MW. 1984. Laser irradiation of centrosomes in newt eosinophils: Evidence of centriole role in motility. J Cell Biol 98:1999–2010.

Kuo Y, Tzeng WL, Li PC, Tang TS, Young ST. 2000. Autostage sperm tracing system for semen evaluation. Arch Androl 44:29–39.

Lang MJ, Block SM. 2003. LBOT-1: Laser-based optical tweezers. Am J Phys 71:201–215.

Mortimer D. 1994. Practical laboratory andrology. New York: Oxford University Press. 393 p.

Mortimer ST. 1997. A critical review of the physiological importance and analysis of sperm movement in mammals. Hum Reprod Update 3:403–439.

Nascimento J, Botvinick EL, Shi LZ, Durrant B, Berns MW. Analysis of sperm motility using optical tweezers. J Biomed Opt, in press.

Neil JM, Old-Clarke P. 1987. A computer-assisted assay for mouse sperm hyperactivation demonstrates that bicarbonate but not bovine serum albumin is required. Gamete Res 18:121–140.

Poole PS, Sinclair DR, Armitage JP. 1988. Real time computer tracking of free-swimming and tethered rotating cells. Anal Biochem 175:52–58.

Rabut G, Ellenberg J. 2004. Automatic real-time three-dimensional cell tracking by fluorescence microscopy. J Microsc 216:131–137.

Sage D, Neumann FR, Hediger F, Gasser SM, Unser M. 2005. Automatic tracking of individual fluorescence particles: Application to the study of chromosome dynamics. IEEE Trans Image Process 4:1372–1383.

Stephens DT, Hickman R, Hoskins DD. 1988. Description, validation, and performance characteristics of a new computer-automated sperm motility analysis system. Biol Reprod 38:577–586.

Tadir Y, Wright WH, Vafa O, Ord T, Asch RH, Berns MW. 1989. Micromanipulation of sperm by a laser generated optical trap. Fertil Steril 52:870–873.

Young ST, Tzeng WL, Kuo YL, Ksiao ML, Chiang SR. 1996. Real-time tracing of spermatozoa. IEEE Eng Med Biol Mag 15:117–120.